J Mater Sci (2011) 46:7582–7587
DOI 10.1007/s10853-011-5733-z

Local inhomogeneity and surface degradation of $Fe_{1.15}Te$ and $Fe_{1.03}Te_{0.62}Se_{0.38}$ single crystals

S. V. Rajasekaran · T. Tite · Y.-M. Chang · R. Sankar · F. C. Chou

Received: 13 January 2011 / Accepted: 21 June 2011 / Published online: 12 July 2011

Abstract We have investigated the structural and magnetic properties of $Fe_{1.15}Te$ and $Fe_{1.03}Te_{0.62}Se_{0.38}$ single crystals grown by slow cooling method using a specially designed double-walled quartz ampoule. X-ray diffraction reveals significant local inhomogeneity as a result of fractional substitution of Te site by Se in single crystal $Fe_{1.03}Te_{0.62}Se_{0.38}$. The existence of superconductivity is confirmed for Se substitution to the Te site of $Fe_{1.03}Te_{0.62}Se_{0.38}$ but with persistent Fe_7Se_8 impurity phase. Raman spectroscopy confirmed the surface structural instability when the samples were exposed to moderate laser irradiation in the atmospheric environment. With high intensity laser irradiation, Fe(Se,Te) compounds can be decomposed into Fe_2O_3 hematite phase.

Introduction

Extensive research has been focused on iron pnictide-layered superconductor since the discovery of superconductivity (SC) in F-doped LaFeAsO of $T_c \sim 26$ K in 2008 [1]. The reason for the SC in iron pnictide superconductors can be described as two kinds of layered building blocks, one is the charge reservoir layer of $[LaO]^+$ and the other is charge accepter layer [2] of $[FeAs]^-$. Subsequently, the findings of SC in iron chalcogenide ($FeSe_{1-x}$) have motivated for research on Fe-based materials further [3]. There is no clear charge reservoir layer in-between the tetrahedrally coordinated Fe–Se layers. Even though both FeTe and FeS are not superconductors at ambient pressures, SC can be induced by Se and S substitutions as in $FeTe_{1-x}Se_x$ and $FeTe_{1-x}S_x$. This seems to assume that the Se deficiency or Fe excess to be necessary to induce SC [4–7]. In particular, the iso-valent substitution does not directly introduce extra carriers but may have changed the topology of the Fermi surface as similar to carrier-doped $LaFeAsO_{1-x}F_x$ (1111) and $BaFe_2As_2$ (122) type superconductors [1, 2, 8].

The interplay of magnetism and SC is a fundamental problem in condensed matter physics and it has been studied experimentally and theoretically for almost four decades. Recent reports on iron pnictide indicate strong correlation between Spin Density Wave (SDW) and SC [1, 2]. Recent studies on iron chalcogenide polycrystalline $FeTe_{0.82}$ shows an anomaly near $T_s = 65$ K [4]. Just below T_s, the system undergoes a structural transition from a high-temperature tetragonal (*P4/nmm*) phase to an orthorhombic (*Pmmn*) phase, where antiferromagnetic ordering has been observed through neutron diffraction study [9, 10]. However, the antiferromagnetic ordering vector **Q** found in iron chalcogenide is different to that found in iron pnictide, where the former cannot be explained as due to the occurrence of SDW by the nesting scenario of Fermi surface in the itinerant picture [9]. In addition, more and more evidence has been accumulated on the local inhomogeneity in the iron chalcogenide system [11, 12]. This is being one of the possible explanations on the origin of SC in high T_c cuprate system [13]. Considering the strong connection between the chemical inhomogeneity and SC found in the superconducting Fe(Te,Se) system, it is suggested that a more detailed analysis of local structural properties through integrated X-ray and Raman scattering studies on good quality of iron chalcogenide crystal is necessary. Herein, we report the crystal growth,

S. V. Rajasekaran · T. Tite · Y.-M. Chang · R. Sankar · F. C. Chou (✉)
Center for Condensed Matter Sciences,
National Taiwan University, Taipei 10617, Taiwan
e-mail: fcchou@ntu.edu.tw

F. C. Chou
National Synchrotron Radiation Research Center,
Hsinchu 30076, Taiwan

Raman, and magnetic property studies of $Fe_{1.15}Te$ and $Fe_{1.03}Te_{0.62}Se_{0.38}$ single crystals grown from an improved melt growth method with identical growth conditions.

Experimental

Fe and (Se,Te) powder was thoroughly mixed in stoichiometric molar ratio of $FeTe_{0.80}$ and $Fe(Te_{0.6}Se_{0.4})_{0.80}$ and ground inside the glove box to avoid oxidation [14]. The pelletized powder was loaded with a quartz tube, and then the tube was flushed with Argon following with evacuation (10^{-3} to 10^{-4}) for several times before sealing. The encapsulated tube was then heated at 800 °C for over 10 h and slowly cooled to room temperature. The sintered pellets were again ground, pelletized, and sealed in a double-walled ampoule. Sample was heated to 910 °C and soaked for about 30 h to get a homogeneous mixture and then ramped down to 400 °C for 40 h.

The obtained single crystal samples were ground into powders for performing powder X-ray diffraction (XRD) using Bruker D8 diffractometer, and the chemical analysis was performed using Electron Microprobe Analysis (EPMA). DC magnetic susceptibilities were measured using Quantum Design Magnetometer (SQUID-MPMS). Micro-Raman measurements were carried out in backscattering configuration at room temperature in atmospheric environment using a 632.8 nm He–Ne laser as an excitation source. In order to avoid any possible laser-induced oxidation effect, the intensity of the laser beam was intentionally set to 6×10^4 W cm^{-2}. An Olympus Plan-N 20X NA0.4 objective was used for laser focusing and Raman signal collection. The thermal properties of the samples were investigated using a 532 nm Neodymium-doped Yttrium Aluminum garnet (Nd:YAG) laser as excitation source and an Olympus 100X NA0.9 objective for laser focusing and Raman signal collection. The spatial and the spectral resolution of this micro-Raman system were estimated to be about 1 μm and 1 cm, respectively. The polarization of the incident and scattered light were adjusted via two pairs of half-wave plate and polarizer. Two polarization configurations were assigned. They are denoted as $\parallel$ and $\perp$, where $\parallel$ and $\perp$ represents the incident light and the scattered light having parallel and perpendicular polarization, respectively. The scattered Raman signal was measured with a Jobin–Yvon FHR640 spectrometer and liquid nitrogen cooled charge-coupled device (CCD).

Results and discussion

Single crystals were grown by an improved melt growth technique using a vertical two-zone tubular furnace. A double-walled ampoule, to avoid the occurrence of oxidation caused by leaks created by a stress-induced crack on the evacuated quartz tube during cooling is shown in Fig. 1a. The distance between the inner and outer tubes is vital for successful growth. After reaching the melting point, the melt leaks from the inner tube and fills the annular space between the inner and outer tubes. A hole in the middle of the inner tube reduces the high vapor pressure during melting. The space above the melt level acts as a thermal insulator due to vacuum [15]. A capillary of about 0.5–1 mm at the lower end of the tube prevents the thermal shock to the inner tube during growth. The crystals were found to be shiny as shown in Fig. 1b and very easy to cleave along the ab-plane.

The cleaved crystals were plate-like and the real compositions were analyzed by EPMA measurements as listed in Table 1. Chemical analysis of crystals grown from the $FeTe_{0.80}$ and $Fe(Te_{0.6}Se_{0.4})_{0.80}$ stoichiometric melt was performed using EPMA to be $Fe_{1.15}Te$ and $Fe_{1.03}Te_{0.62}Se_{0.38}$, respectively. Result shows that the number of Fe atoms incorporated into the crystal structure decreases by Se doping and the observed Se content was found lesser than the nominal one. In general, the excess Fe in FeTe compared with

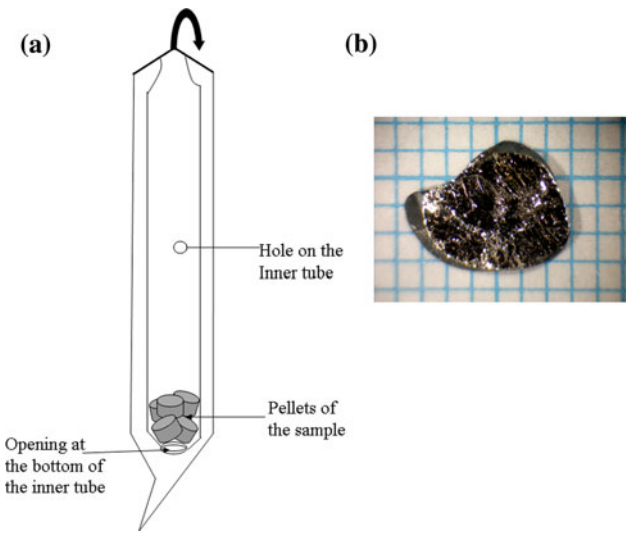

Fig. 1 **a** Schematic diagram of a sealed double-walled ampoule. The inner wall has two openings, one is at the bottom and the other is at the side. **b** Photo of single crystal $Fe_{1.15}Te$

Table 1 Nominal and measured (EPMA) compositions of the samples used for this study

Sample (nominal)	Fe (observed)	Te (observed)	Se (observed)
$FeTe_{0.80}$	1.15	1	0
$Fe(Te_{0.6}Se_{0.4})_{0.80}$	1.03	0.62	0.38

FeSe may retain its metallic state at low temperature even under high pressure unlike FeSe, which turns as a superconductor [16]. So, the induction of SC indicates that there is a lattice disorder in the superconducting Fe layer due to Se substitution in Te site, which is contrary to layered cuprate superconductors where doping onto the Cu sublattice. The disordered vacancies of Fe site in $FeTe_{0.62}Se_{0.32}$ may lead to lattice disorder as in $Zr_{1-x}S$ where vacancies are from the Zr sites for large x and on both Zr and S sites [17] for smaller x. XRD measurements were done on fresh pieces of $Fe_{1.15}Te$ and $Fe_{1.03}Te_{0.62}Se_{0.38}$ to reveal preferred orientation of {00l} and perpendicular to the ab-plane (Fig. 2a). Powder XRD could be well indexed on the basis of tetragonal PbO-type structure with space group *P4/nmm*. Lattice parameters were fitted to be $a = 3.8280$ Å and $c = 6.2640$ Å for $Fe_{1.15}Te$ and $a = 3.7980$ Å and $c = 6.0580$ for $Fe_{1.03}Te_{0.62}Se_{0.38}$, which

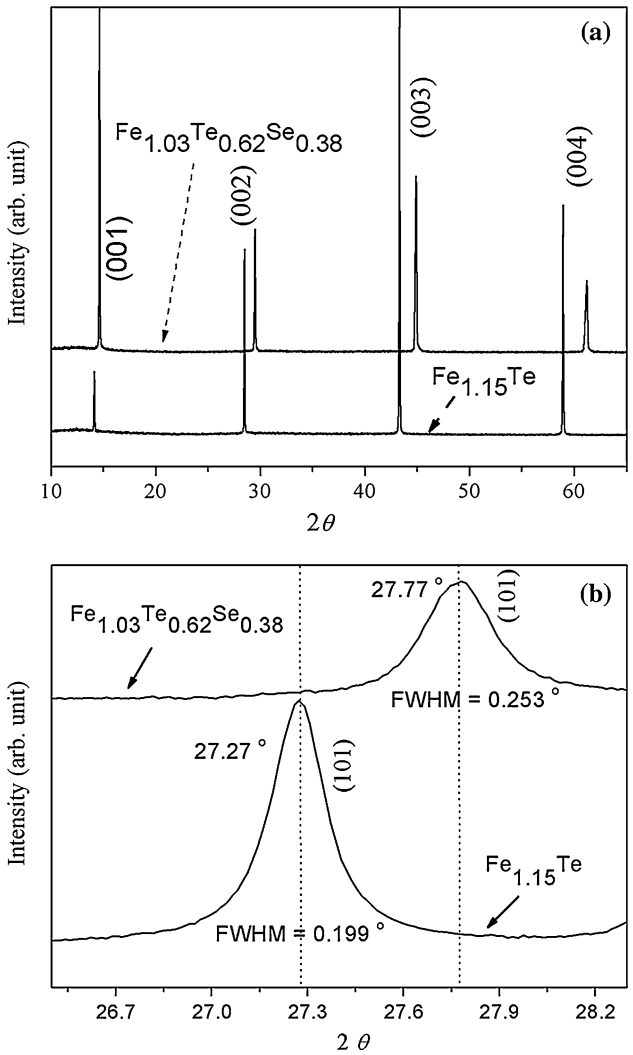

Fig. 2 **a** X-ray diffraction pattern of plane of single crystals $Fe_{1.15}Te$ and $Fe_{1.03}Te_{0.62}Se_{0.38}$ and **b** Comparison of diffraction peaks of (101)

are in good agreement with those reported in the literature [4, 9]. Weak secondary phase Fe_7Se_8 can be identified in $Fe_{1.03}Te_{0.62}Se_{0.38}$. Although $Fe_{1.03}Te_{0.62}Se_{0.38}$ crystal shows equally shiny surface quality as that of $Fe_{1.15}Te$, its XRD pattern reveals relatively poor crystallinity when comparing the FWHM for these two samples (Fig. 2b). Considering the near identical amount of chalcogen vacancy level and growth condition, the most probable origin of this significant XRD peak broadening is a reflection of local structural inhomogeneity as a result of compositional inhomogeneity between Te and Se. While $Fe_{1.15}Te$ has only Te vacancy or alternatively Fe excess, $Fe_{1.03}Te_{0.62}Se_{0.38}$ must possess additional factor from the random distribution of Se of smaller ion size to create more local inhomogeneity.

Results of the magnetic susceptibility measurements are shown in Fig. 3. $Fe_{1.15}Te$ undergoes a transition from paramagnetic to antiferromagnetic phase near 70 K and a high-temperature Curie–Weiss behavior is observed (Fig. 3a). In addition to the antiferromagnetic transition, we observed a significant ZFC/FC hysteresis immediately below the onset of the AF transition temperature. Recent neutron diffraction study on $Fe_{1.141}Te$ indicates the existence of antiferromagnetic ordering with an in-plane propagation vector along the diagonal direction of the Fe-sublattice [9]. In addition, a high-temperature tetragonal *P4/nmm* to low temperature *Pmmn* orthorhombic structure transition follows. In our case, the magnetic hysteresis found immediately below the AF transition ($\sim$70 K) suggests that irreversible domains are present during the tetragonal to orthorhombic structure transition, while the antiferromagnetic ordering stabilizes in orthorhombic symmetry only, as required partly by the incommensurability of the propagation vector [9].

For the magnetic susceptibilities of $Fe_{1.03}Te_{0.62}Se_{0.38}$ as shown in Fig. 3b, there is an enhanced anomaly found near 130 K. Magnetic impurities such as Fe_7Se_8 [3, 18–20] and Fe_3O_4 [4] have been suggested to be hard to avoid during the preparation of Fe(Te,Se) samples. While Verwey transition for Fe_3O_4 occurs around 120 K, the anomaly at 130 K suggests the presence of Fe_7Se_8 impurity with a spin-axis transition at $\sim$130 K [8, 21], which is in agreement with our finding of Fe_7Se_8 from the XRD analysis. The data displayed in the inset of Fig. 3b indicates that the as-grown $Fe_{1.03}Te_{0.62}Se_{0.38}$ crystal to be superconducting with a $T_c \sim 12$ K. However, even zero-field-cooled (ZFC) superconducting screening level is approaching 70%, flux pinning due to the existence of Fe_7Se_8 impurity phase leads to a significantly reduced field-cooled Meissner effect as indicated by the FC data.

Since tetragonal $Fe_{1+x}(Te,Se)$ crystal belongs to the space group of *P4/nmm* and point group D_{4h}^7, there are four expected Raman-active optical modes: A_{1g}(Te), B_{1g}(Fe), E_g(Te), and E_g(Fe), where the E_g mode is two-fold

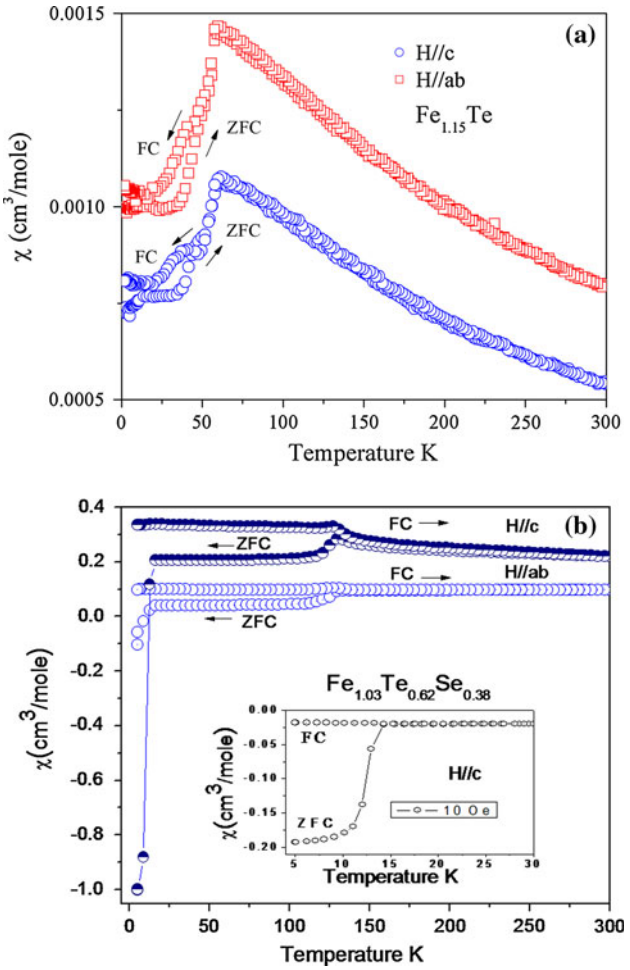

Fig. 3 Magnetic susceptibilities for **a** $Fe_{1.15}Te$ and **b** $Fe_{1.03}Te_{0.62}Se_{0.38}$ at $H = 300$ Oe and 10 Oe (inset of **b**). Note the anomaly near 130 K shown in **b** corresponds to the spin-axis transition of the Fe_7Se_8 impurity phase

degenerate [22]. According to the Raman selection rules derived from the group theory, only A_{1g} and B_{1g} modes are measurable when the experiment is performed in backscattering configuration along the *z*-axis (i.e., [001] direction). Xia et al. reported the polarized Raman spectroscopy of $FeTe_{0.92}$ and $Fe_{1.03}Se_{0.30}Te_{0.70}$ single crystals in the cryostat and vacuum environment [22]. Two Raman peaks at ~ 159 and ~ 196 cm^{-1} for $FeTe_{0.92}$ were assigned to the A_{1g}(Te) and B_{1g}(Fe) phonon modes, respectively. However, the A_{1g}(Te) mode was absent in the Raman spectrum of superconducting sample $Fe_{1.03}Se_{0.30}Te_{0.70}$. Recently, Okazaki et al. reported the Raman study of $Fe_{1.074}Te$ and $FeTe_{0.6}Se_{0.4}$ at various temperatures [23]. In $Fe_{1.074}Te$, the frequencies of A_{1g}(Te) and B_{1g}(Fe) modes measured at 5 K were reported to be 157.5 and 202.3 cm^{-1}, respectively [23].

Figure 4 shows typical Raman spectra of (a) $Fe_{1.15}Te$ and (b) $Fe_{1.03}Te_{0.62}Se_{0.38}$ performed in the room temperature with atmospheric environment. Here, 632.8 nm He–Ne laser was used as an excitation light source and low laser intensity (6×10^4 W cm^{-2}) was used to avoid any possible thermal effect. The Raman peaks were found to be sensitive to both the polarization configuration and the crystal orientation. Indeed, a weak Raman peak at ~ 200 cm^{-1} in the spectra (indicated by arrows in Fig. 4a and b) can be attributed to the expected B_{1g}(Fe) phonon modes [23]. However, two additional Raman peaks at ~ 121 and ~ 141 cm^{-1} in fact dominate the Raman spectra. Meanwhile the Raman spectra were further measured at different sample spots to investigate the issue of the local inhomogeneity of these two samples and are shown in Fig. 4c and d. The sample surface was shiny with no distinguishable domain structure when viewed with an optical microscope. In particular, the two dominant peaks were found to be slightly shifted in frequency (between $121 \sim 125$ and 141–144 cm^{-1}) and broadened for some sample spots. These two modes are not expected in the vibrational spectra of Fe(Se,Te) compounds[22–24]. It is worthy to note that these two modes were still observable even for freshly cleaved crystal samples. The frequencies for the observed Raman spectra at $\sim 121 \pm 4$ and 141 ± 3 cm^{-1} match very well with the A_1 (119–121 cm^{-1}) and E (139–142 cm^{-1}) modes of crystalline tellurium (c-Te) [25–27]. By increasing the degree of disorder, the Raman modes of c-Te are expected to shift to higher frequencies [26, 28]. Our Raman measurement results reveal the coexistence of c-Te either in the precipitate or surface layer of $Fe_{1.15}Te$ and $Fe_{1.03}Te_{0.62}Se_{0.38}$ crystals. In fact, our Raman spectra show great similarity to those reported in the work of Xia et al. [22], when their samples were intentionally exposed to air for days or exposed to laser beam for a short time.

The structural and thermal instability of the FeTe-based material is not fully understood up to now. Here, we are giving a tentative explanation regarding the formation of tellurium in our samples. Some previous Raman studies have reported that laser could induce the tellurium enrichment in CdTe compounds [29, 30], which suggests that a similar mechanism may have occurred in our case. In fact, the presence of elemental tellurium phases in the Raman spectra of many telluride compounds has been well established nowadays [28, 29, 31, 32]. Assisted by a fragile structure and easily breakable Fe-(Te,Se) bonds [33], temperature gradient at the crystal surface would induce thermal migration of Te atoms to form c-Te cluster [29], although the possibility of micro-Te clusters formation inside the grain boundary during the melt growth cannot be ruled out completely [33].

As shown in Fig. 5, we find that the Raman spectrum of $Fe_{1.15}Te$ can change completely under a moderate laser intensity irradiation (1.20×10^6 W cm^{-2}) in the atmospheric environment. The emergence of new peaks in the Raman spectrum is indicative of a laser-induced heating

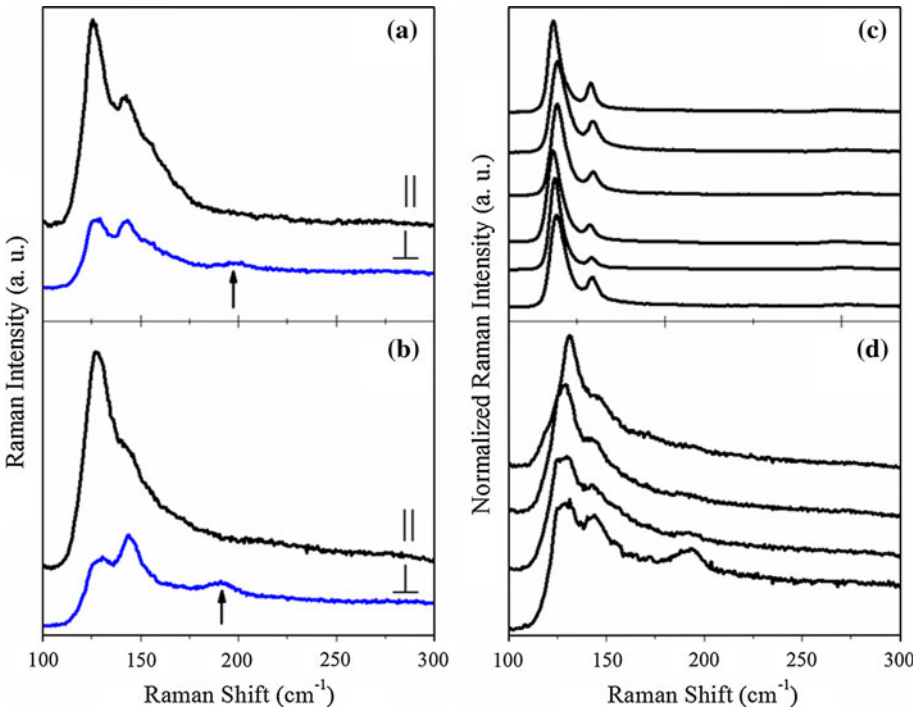

Fig. 4 Raman spectra of **a** $Fe_{1.15}Te$ and **b** $Fe_{1.03}Te_{0.62}Se_{0.38}$ measured with a low laser intensity (6×10^4 W cm^{-2}) under two polarization configurations (∥ or ⊥). Here 632.8 nm He–Ne laser was used as the excitation light source; **c** and **d** show some Raman spectra measured at different sample spots of $Fe_{1.15}Te$ and $Fe_{1.03}Te_{0.62}Se_{0.38}$, respectively

effect in the structure. After the moderate laser exposure, the Raman spectrum was measured again at low laser intensity (i.e., 3.0×10^5 W cm^{-2}) to examine the structural property of the sample (spectrum d of Fig. 5). The Raman peaks associated with Te-phase and $Fe_{1.15}Te$ are totally gone and some additional phonon peaks can be resolved now. This spectrum change indicates a laser-induced decomposition process of the $Fe_{1.15}Te$ sample.

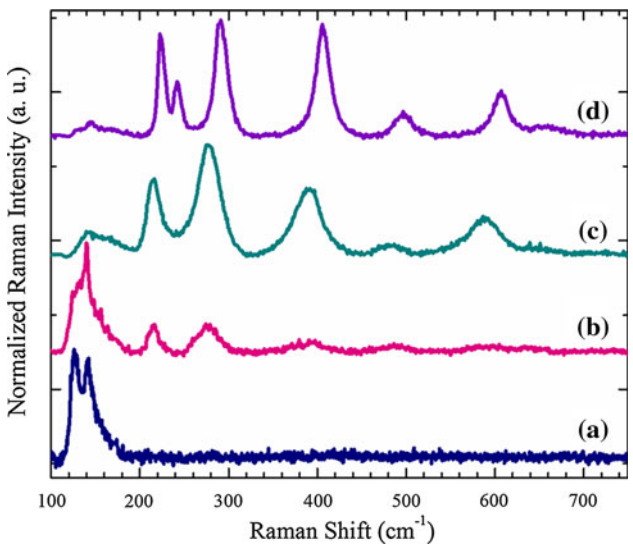

Fig. 5 Normalized Raman spectra of $Fe_{1.15}Te$ measured in the following laser intensity sequence: (*a*) 3.0×10^5 W cm^{-2}, (*b*) 6.0×10^5 W cm^{-2}, (*c*) 1.2×10^6 W cm^{-2}, and (*d*) 3.0×10^5 W cm^{-2}. Here 532 nm Nd:YAG laser was used as the excitation light source

This process leads to the generation of a new phase, which was identified as the hematite phase [34] Fe_2O_3. A similar result was observed for $Fe_{1.03}Te_{0.62}Se_{0.38}$. We argue that this phase transition is an oxidation process induced by the laser heating effect in the atmospheric environment.

Conclusions

We have presented a double wall sealed quartz tube design for the melt crystal growth of Fe(Te,Se). Physical properties of the sizable crystals up to $5 \times 5 \times 2$ mm^3 have been studied using XRD, magnetic susceptibility, and Raman spectroscopy. Local inhomogeneity is implied to exist in $Fe_{1.03}Te_{0.62}Se_{0.38}$ single crystal from both the Raman and XRD results. Irreversible domain boundary formation due to the competing tetragonal and orthorhombic phases has been revealed by the magnetic thermal hysteresis in $Fe_{1.15}Te$ below the antiferromagnetic ordering temperature also. The Fe(Te,Se) surface can easily deteriorate and become Te-rich phase due to the sample's exposure to the atmospheric environment for a few days or by moderate laser irradiation. Due to higher intensity of laser irradiation, Fe(Se,Te) compounds become thermally unstable in air and were found to change into Fe_2O_3 hematite phase. This surface degradation and phase transition phenomena were confirmed by Raman spectroscopy.

Acknowledgement FCC acknowledges the support from National Science Council of Taiwan under project number NSC-99-2119-M-002-011-MY2.

Reference

1. Kamihara Y, Watanabe T, Hirano M, Hosono H (2008) J Am Chem Soc 130:3296
2. Johnston DC (2010) Adv Phys 59:803
3. Hsu FC, Luo JY, Yeh KW, Chen TK, Huang TW, Wu PM, Lee YC, Huang YL, Chu YY, Yan DC, Wu MK (2008) Proc Natl Acad Sci 105:14262
4. Fang MH, Pham HM, Qian B, Liu TJ, Vehstedt EK, Liu Y, Spinu L, Mao ZQ (2008) Phys Rev B 78:224503
5. Sales BC, Sefat AS, McGuire MA, Jin RY, Mandrus D (2009) Phys Rev B 79:094521
6. Chen GF, Chen ZG, Dong J, Hu WZ, Li G, Zhang XD, Zheng P, Luo JL, Wang NL (2009) Phys Rev B 79:140509
7. Mizuguchi Y, Tomioka F, Tsuda S, Yamaguchi T, Takano Y (2009) Appl Phys Lett 94:012503
8. Christianson AD, Goremychkin EA, Osborn R, Rosenkranz S, Lumsden MD, Malliakas CD, Todorov IS, Claus H, Chung DY, Kanatzidi MG, Bewley RI, Guidi T (2008) Nature 456:930
9. Bao W, Qiu Y, Huang Q, Green MA, Zajde P, Fitzsimmons MR, Zhernenkov M, Chang S, Fang M, Qian B, Vehstedt EK, Yang J, Pham HM, Spinu L, Mao ZQ (2009) Phys Rev Lett 102:247001
10. Li S, Cruz C, Huang Q, Chen Y, Lynn JW, Hu J, Huang YL, Hsu FC, Yeh KW, Wu MK, Dai P (2009) Phys Rev B 79:054503
11. Joseph B, Iadecola A, Puri A, Simonelli L, Mizuguchi Y, Takano Y, Saini NL (2010) Phys Rev B 82:020502
12. Hu H, Zuo JM, Wen JS, Xu ZJ, Lin ZW, Li Q, Gu G, Park WK, Greene LH, arXiv:1009.6010v1
13. Eroles J, Ortiz G, Balatsky AV, Bishop AR (2000) Europhys Lett 50:540
14. Chiba S (1955) J Phys Soc Jpn 10:837
15. Balamurugan N, Arulchakkaravarthi A, Ramasamy P (2008) J Cryst Growth 310:2115
16. Okada H, Takahashi H, Mizuguchi Y, Takano Y, Takahashi H (2009) J Phys Soc Jpn 78:083709
17. Moodenbaugh AR, Johnston DC, Viswanathan R, Shelton RN, DeLong LE, Fertig WA (1978) J Low Temp Phys 33:175
18. McQueen TM, Huang Q, Ksenofontov V, Felser C, Xu Q, Zandbergen H, Hor YS, Allred J, Williams AJ, Qu D, Checkelsky J, Ong NP, Cava RJ (2009) Phys Rev B 79:014522
19. Williams AJ, McQueen TM, Cava RJ (2009) Solid State Commun 149:1507
20. Bendele M, Weyeneth S, Puzniak R, Maisuradze A, Pomjakushina E, Conder K, Pomjakushin V, Luetkens H, Katrych S, Wisniewski A, Khasanov R, Keller H (2010) Phys Rev B 81:224520
21. Okazaki A, Hirakawa K (1956) J Phys Soc Jpn 11:930
22. Hou TLD, Zhao SC, Zhang AM, Chen GF, Luo JL, Wang NL, Wei JH, Lu ZY, Zhang QM (2009) Phys Rev B 79:140510
23. Okazakil K, Sugai S, Niitaka S, Takagi H (2011) Phys Rev B 83:035103
24. Kumar P, Kumar A, Saha S, Muthu D, Prakash J, Patnaik S, Waghmare U, Ganguli A, Sood A (2010) Solid State Commun 150:557
25. Torrie BH (1970) Solid State Commun 8:1899
26. Morell G, Figueroa AR, Katiyar RS, Farías MH, Beltran FJE, Angel OZ, Sinencio FS (1994) J Raman Spectrosc 25:203
27. Pine AS, Dresselhaus G (1971) Phys Rev B 4:356
28. Andrikopoulos KS, Yannopoulos SN, Voyiatzis GA, Kolobov AV, Ribes M, Tominaga J (2006) J Phys Condens Matter 18:965
29. Hawkins SA, Aleman EV, Duff MC, Hunter DB, Burger A, Groza M, Buliga V, Black DR (2008) J Electron Mater 37(9):1438
30. Teuchert WD, Geick R (1974) Phys Status Solidi (b) 61:123
31. Bastiani RD, Carria E, Gibilisco S, Grimaldi MG, Pennisi AR, Gotti A, Pirovano A, Bez R, Rimini E (2009) Phys Rev B 80:245205
32. Larramendi EM, Berth G, Wiedemeier V, Husch KP, Zrenner A, Woggon U, Tschumak E, Lischka K, Schikora D (2010) Semicond Sci Technol 25:075003
33. Okamoto H (1990) Bull Alloy Phase Diagr 4(11):372
34. Shebanova ON, Lazor P (2003) J Raman Spectrosc 34:845